

Observations of High Energy Electrons during the 5 September 2022 Solar Energetic Particle Event with the Parker Solar Probe EPI-Hi Instrument

A.W. Labrador^{a,*}, J.G. Mitchell^b, E.R. Christian^b, C.M.S. Cohen^a, A.C. Cummings^a,
G.A. de Nolfo^b, R.A. Leske^a, D.J. McComas^c, R. A. Mewaldt^a, J.S. Rankin^{a,c}, N. Schwadron^d,
E.C. Stone^a, J. Szalay^d, M.E. Wiedenbeck^c

^a California Institute of Technology, Pasadena, CA, USA 91125

^b NASA/Goddard Space Flight Center, Greenbelt, MD, USA 20771

^c Department of Astrophysical Sciences, Princeton University, Princeton, NJ, USA 08544

^d University of New Hampshire, Durham, NH, USA 03824

^e Jet Propulsion Laboratory, California Institute of Technology, Pasadena, CA, USA 91109

* E-mail: labrador@srl.caltech.edu

The 5 September 2022 SEP event observed by Parker Solar Probe yielded some of the highest intensities in high energy electrons observed at the instrument since its launch in 2018. For this paper, we will examine the high energy electron signals detected by the EPI-Hi HET instrument to measure the spectra, the time-evolution of the spectra, and anisotropies in electrons during the event. We will examine the HET electron measurements and compare them with the proton measurements. We will also explain in detail the calculation of the electron spectra during periods of very high count rate.

38th International Cosmic Ray Conference (ICRC2023)
26 July - 3 August, 2023
Nagoya, Japan



* Speaker

© Copyright owned by the author(s) under the terms of the Creative Commons Attribution-NonCommercial-NoDerivatives 4.0 International License (CC BY-NC-ND 4.0).

<https://pos.sissa.it/>

1. Introduction

Since Parker Solar Probe was launched in 2018, the Integrated Science Investigations of the Sun (IS \odot IS) suite has successfully reported observations of several SEP events (e.g. [1], [2], [3], [4], [5], [6], [7], [8], and [9]), while approaching closer to the solar surface with successive orbits. The IS \odot IS suite of energetic particle detectors ([10]) aboard Parker Solar Probe contains two components: EPI-Lo, which measures ions at ~ 20 keV/nuc to 15 MeV total energy and electrons from ~ 25 keV to 1 MeV, and EPI-Hi, which measures ions at ~ 1 -200 MeV/nuc and electrons from ~ 0.5 to ~ 6 MeV. EPI-Hi itself consists of three telescopes (designated HET, LET1, and LET2) of stacked solid-state detectors ([10], [11]) which use the dE/dx vs. E' technique to identify ions. HET is composed of 16 solid-state detectors in a double-ended configuration (A-side and B-side). LET1 is a similarly double-ended stack of 10 solid-state detectors, and LET2 is a single-ended configuration of 7 stacked solid-state detectors. As described in [11], the three telescopes are aligned in three different directions relative to the spacecraft and cover slightly different energy ranges, with HET going up to ~ 6 MeV for electrons, the highest energy range of the three. In this paper, we will focus on electron and proton analysis with HET data. The HET telescope has more guard rings than the LET telescopes, making the electron results cleaner for HET than for the LETs.

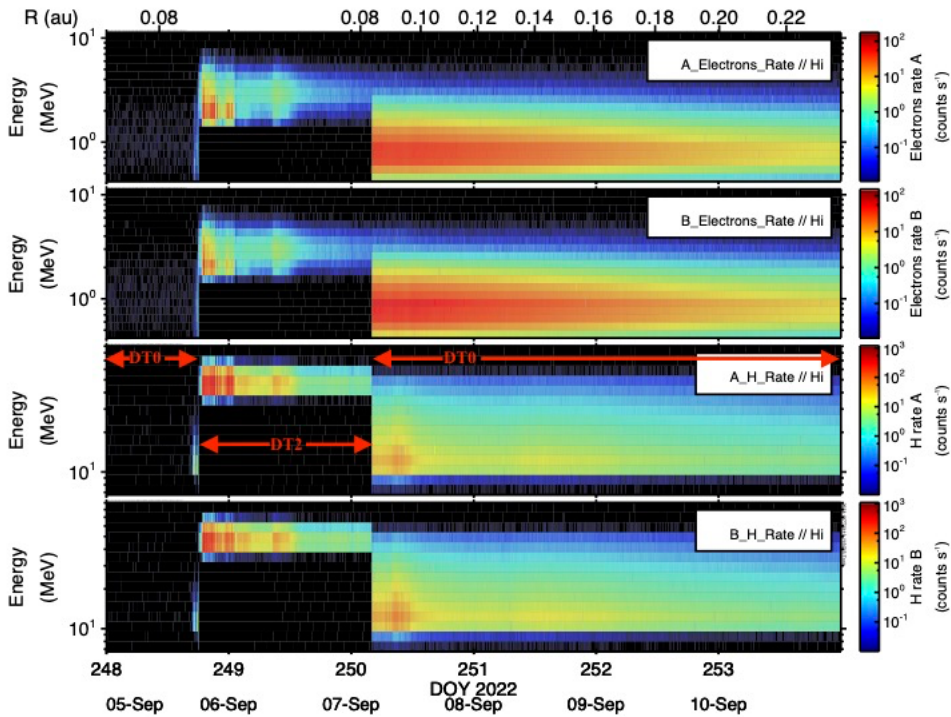


Figure 1: Spectrograms measured by EPI-Hi HET for electrons (top two panels) and protons, on the A and B sides of the instrument. Time periods for normal trigger (DT0) and dynamic threshold state 2 (DT2) are marked on the A_H_Rate panel for this event.

On 5 September 2022, a very large SEP event was observed by Parker Solar Probe while the spacecraft was at 0.08 au and traveling out to ~ 0.36 au. Figure 1 shows electron and proton spectrograms measured by EPI-Hi HET for the event. The event started around 17:00 on 5 September 2022. The particle intensities rose rapidly, triggering a dynamic threshold mode in EPI-Hi HET just after 18:00, to reduce low Z singles rates and instrument dead time. The dynamic threshold mode reduces singles rates by raising the pulse height thresholds on the three outermost detector layers on each side of the telescope, so that the three outer layers are sensitive to only particles at $Z \geq 6$. The dynamic threshold state is marked on the figure by the absence of the lowest energy particles, e.g. below 1.4 MeV measured in the instrument for electrons.

The particle intensities reached maximum around 20:00 in both electrons and protons, and the instrument stayed in the dynamic threshold mode (DT2, or dynamic threshold state 2) until returning to normal triggering (DT0) around 04:00 on 7 September 2022. The instrument remained in normal triggering mode through the end of the event, around 15 September 2022.

2. Electron Spectrum Analysis

To separate particles by charge, mass, and energy, one plots the measured energy deposited by a charged particle passing through one solid state detector vs. the energy deposited by the particle stopping in the next, adjacent detector. This technique has been in use in solid-state detector telescopes in space missions for decades (e.g. ACE CRIS and SIS, [12], [13]). The technique is illustrated in Figure 2, showing simulated dE/dx vs. E' plots for various adjacent detector pairs in the HET detector stack, for protons and electrons stopping in the lower of the two detectors. Protons show well-defined curves in the four panels, with higher incident energies corresponding to deeper penetration in the stack as well as moving farther to the right in each individual panel. Heavier ions would show similar tracks parallel to the proton track and higher on the deposited energy scales.

However, because they are much less massive, electrons are far more likely to scatter out of any individual layer as well as to scatter back into a layer after interacting with the surrounding material (e.g. the telescope body or the detector mounting materials), they may scatter into annular guard rings surrounding the detector active areas and trigger anticoincidence, or they may scatter and leave the telescope entirely without depositing all of their energy. As a result, electrons deposit less energy compared to ions to a given penetration range within the detector stack, their dE/dx vs. E' measurements do not exhibit the same well-defined tracks in the figures, and their incident energies are therefore more difficult to determine directly.

We use a response matrix approach to estimating energetic electron spectra, using Geant4 simulations of each of the detectors. The response matrix approach described herein is similar to that used to calibrate the electron responses on the Caltech Electron/ Isotope Spectrometer (EIS) aboard IMP 7 [14]. The earlier work used used beta spectrometer calibration data rather than simulations.

This analysis uses the Geant4 library ([15]) to construct a model of the EPI-Hi HET telescope and to simulate its response to incident energetic electrons. The simulation includes physical description of the telescope, including the silicon wafers (active areas, inactive areas, and guard rings used to reject particles escaping the telescope), detector mounts, windows, and aluminum housing. Test particles (e.g. electrons, protons) are simulated with isotropic incidence

and varying kinetic energies entering the telescope through an the outermost window. The Geant4 code simulates ionization energy losses and energy deposited in all materials, scattering, and production of secondary particles. Geometric acceptance is built into the models and the resulting simulations. The HET model is shown in Figure 3. Similar models exist for LET1 and LET2.

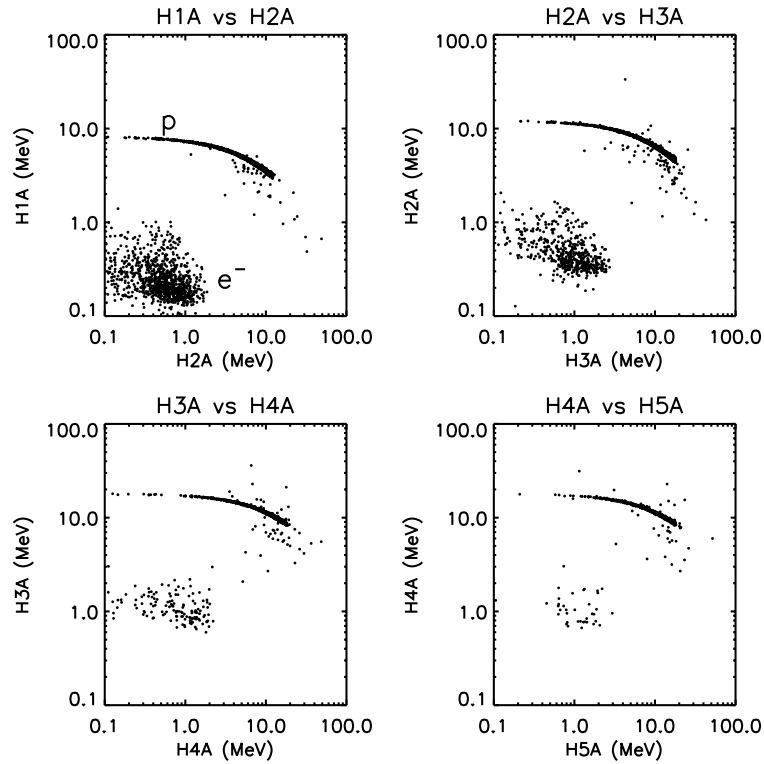


Figure 2: Simulated dE/dx vs. residual energy measurements for protons and electrons at four different penetration ranges in the HET detector stack.

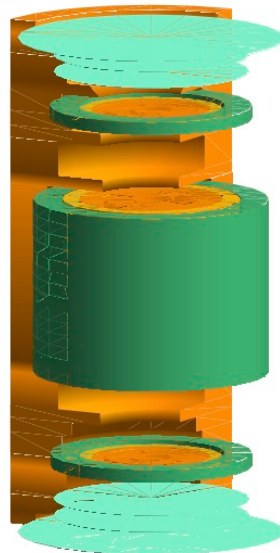


Figure 3: Geant4 drawing EPI-Hi HET. The aluminum body is cut away to 0-90 degrees to show the interior detector configurations. The Kapton windows are shown in aqua. Active areas of the detector layers are shown in dark orange, while

guard rings are shown in lighter orange. Detector mounts are shown in green. The figures are not shown to scale relative to each other.

A response matrix, P , is created with the simulation by sending test electrons of known energies through the telescope. Energies deposited in each active detector segment are tabulated and summed for a total measured energy for each particle. The simulation approximates the instrument flight software by imposing the same selection criteria used to identify electrons. These selection criteria are that particles penetrating to a given detector fall within a given dE/dx vs. E' box for that layer, that particles trigger each of the preceding detector layers, that detector layers beyond the stopping layer are not triggered, and that no guard rings are triggered.

P_{ij} is the probability that an electron entering the top of the telescope in an energy bin j will be measured within the instrument in an energy bin i , calculated as the sum of energies deposited in all detectors in the instrument while also satisfying the electron selection criteria above. Given the nonzero probability of electrons scattering out of the instrument and depositing less than their incident energies, electrons in incident energy bin j will have a peak in deposited energies at bin $i=j$, but there will also be a significant distribution of electrons in energy bins $i < j$.

Energy bin limits for electrons, measured in the telescope, take the form

$$E_i = 2^{(i-6)/4} \text{ MeV} \quad [1]$$

where i is an integer from 0 to 18 in this analysis. For normal mode (DT0), the six lowest and narrowest energy bins are collected into two bins, for a total of 15 bins, and for the dynamic threshold state (DT2) in this analysis, only the 10 energy bins above 2 MeV outside the instrument (~ 1.4 MeV summed in the instrument) are included. P_{ij} will not sum to 1 for a given input energy due to electrons lost by scattering out of the telescope or rejected for triggering guard rings.

Vector f is constructed from the number of electrons in each energy bin j entering the telescope. The number of electrons reported by the instrument in each energy bin i is represented by a vector r given by

$$r_i = \sum_j P_{ij} f_j \quad [2]$$

Given electron rates r returned by the telescope data, the rates f of electrons entering the instrument would be given by

$$f = P^{-1} r \quad [3]$$

P^{-1} is the inverse of the response matrix P . (In analyzing flight data, r may be either rates or summed counts, which would yield either intensities or fluences, depending on the application.)

Each electron response matrix P is constructed with electron test particles emitted isotropically (2π steradian facing the telescope) from a disk above and slightly larger than the outermost window. For flexibility in re-calculating the matrix, if needed, we simulate electrons in monoenergetic beams distributed evenly across each energy bin E_i , at 4-10 million electrons per energy bin. The energy range of the simulation extends to ~ 20 MeV in order to catch the effect of higher energy electrons being detected as lower energy electrons. Further optimization of the simulation and the response matrix is beyond the scope of this paper.

The response matrices for HET DT0 and DT2 are represented graphically in Figures 4 and 5, as a number density plotted in measured, deposited energy vs. incident energy. The large squares at low energies on the DT0 response matrix are the combined energy bins. The diagonal on the matrix shows that the maximum deposited energy for a given incident energy equals that incident energy, while the distribution below that diagonal demonstrates allowance for energy loss due to scattering out of the detector active areas. For the DT2 matrix — in preliminary form as of this writing — there is an offset between the total energy deposited in the instrument (y-axis) and the incident energy (x-axis) of the particle, e.g. the lowest incident energy is ~ 2 MeV for electrons, corresponding to ~ 1.4 MeV measured by summing the innermost layers. The three outer layers on each side of HET account for some energy loss but are not summed in the instrument measured energy.

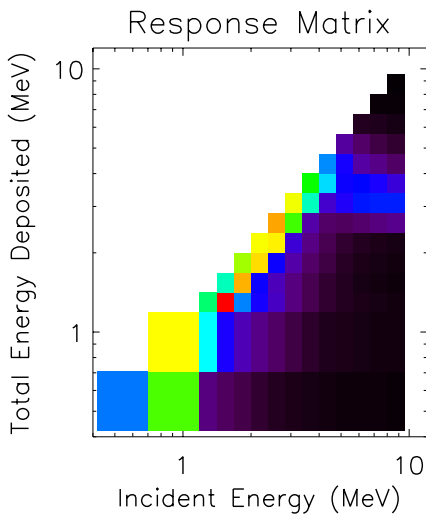


Figure 4: A graphical representation of the HET electron response matrix, normal mode, shown as deposited (measured) energy vs. incident energy.

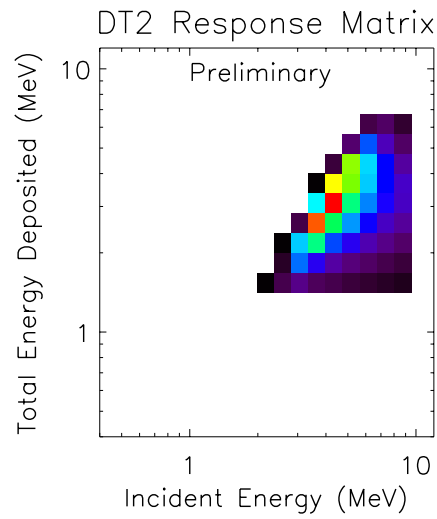


Figure 5: A graphical representation of the preliminary HET electron response matrix, dynamic threshold mode 2 (DT2), shown as deposited (measured) energy vs. incident energy.

3. Spectra for the 5 September 2022 event

Electron spectra for the 5 September 2022 event, measured by EPI-Hi HET, are shown in Figure 6, using the analysis described in section 2. Hourly electron count rates are entered as vector r from Equation 3, and we incorporate for livetime and geometry factor. The event is divided into two time periods: (1) 5 September 2022 19:00 to 7 September 2022 04:00, for DT2, and (2) 7 September 2022 05:00 to 11 September 2022 23:00 for normal mode (DT0), during the long declining tail end of the event. For this paper, the very-brief period of DT0 at the beginning of the event is set aside.

Given the DT2 matrix is still preliminary as of this writing, the spectra for the DT2 portion of the event are similarly set aside. However, Figure 6 shows A- (black) and B-side (red) spectra for HET electron data from the normal mode period of the event (DT0, 9/7/22 05:00 to 9/11/22 23:00). Power law fits to the spectra from ~ 0.9 to ~ 6 MeV are shown, with no strong indication of anisotropy in this data, either in spectral index or in absolute intensities. The proton spectra (not shown) for A and B also show the same power law, albeit of ~ -3.2 for both sides for DT0. Analysis for DT2 with protons is under way.

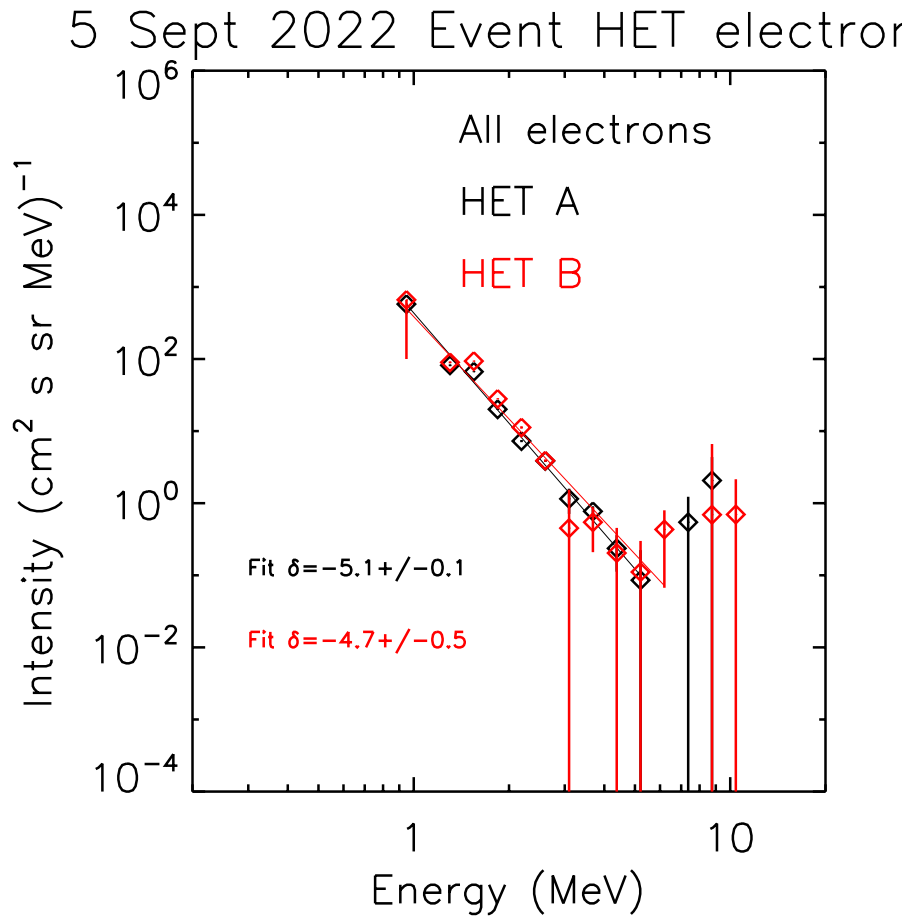


Figure 6: 5 September 2022 energetic electron spectra measured by EPI-Hi HET for the A side (black) and the B side (red) of the instrument, for the tail end of the event (DT0).

4. Summary

We have described proton and electron measurements by the Parker Solar Probe EPI-Hi HET instrument for the 5 September 2022 event. We have described in detail the response matrix approach for calculating electron spectra, including preliminary work with high-intensity, dynamic threshold modes for electrons with the HET instrument.

Acknowledgements: This work was supported by NASA's Parker Solar Probe Mission, contract NNN06AA01C. Parker Solar Probe was designed, built, and is now operated by the Johns Hopkins Applied Physics Laboratory as part of NASA's Living with a Star (LWS) program. Support from the LWS management and technical team has played a critical role in the success of the Parker Solar Probe mission.

References

- [1] Fox, N. J., Velli, M. C., Bale, S. D., et al. 2016, *Space Sci. Rev.*, 204, 7.
- [2] McComas, D. J., Christian, E. R., Cohen, C. M. S., et al. 2019, *Nature*, 576, 223.
- [3] Giacalone, J., Mitchell, D. G., Allen, R. C., et al. 2020, *ApJS*, 246, 29.
- [4] Hill, M. E., Mitchell, D. G., Allen, R. C., et al. 2020, *ApJS*, 246, 65.
- [5] Leske, R.A., Christian, E.R., Cohen, C.M.S., et al., 2020 *ApJS*, 246, 35.
- [6] Mitchell, D. G., Giacalone, J., Allen, R. C., et al. 2020, *ApJS*, 246, 59.
- [7] Schwadron, N. A., Bale, S., Bonnell, J., et al. 2020, *ApJS*, 246, 33.
- [8] Wiedenbeck, M. E., Buc \check{r} ík, R., Mason, G. M., et al. 2020, *ApJS*, 246, 42 .
- [9] Cohen, C. M. S., Christian, E. R., Cummings, A. C., et al. 2021, *A&A*, submitted 275 .
- [10] McComas, D. J., Alexander, N., Angold, N., et al. 2016, *Space Sci. Rev.*, 204, 290, 187.
- [11] Wiedenbeck, M. E., Angold, N. G., Birdwell, B., et al. 2017, in *International Cosmic Ray Conference*, Vol. 301, 35th International Cosmic Ray Conference (ICRC2017), 16 .
- [12] Stone, E. C., Cohen, C. M. S., Cook, W. R., et al. 1998a, *Space Sci. Rev.*, 86, 285 .
- [13] Stone, E. C., Cohen, C. M. S., Cook, W. R., et al. 1998b, *Space Sci. Rev.*, 86, 300, 357 .
- [14] Hurford, G. J., Mewaldt, R. A., Stone, E. C., & Vogt, R. E. 1974, *ApJ*, 192, 541.
- [15] Agostinelli, S., Allison, J., Amako, K., et al. 2003, *Nuclear Instruments and Methods in Physics Research A*, 506, 250. And <http://geant4.web.cern.ch/>